First order reversal curve studies of permanent magnets

Thomas Schrefl, Tetsuya Shoji, Michael Winklhofer, Harald Oezelt, Masao Yano, and Gergely Zimanyi

Citation: Journal of Applied Physics **111**, 07A728 (2012); doi: 10.1063/1.3678434
View online: http://dx.doi.org/10.1063/1.3678434
View Table of Contents: http://scitation.aip.org/content/aip/journal/jap/111/7?ver=pdfcov
Published by the AIP Publishing

First order reversal curve studies of permanent magnets

Thomas Schrefl,[1,a)] Tetsuya Shoji,[2] Michael Winklhofer,[3] Harald Oezelt,[1] Masao Yano,[2] and Gergely Zimanyi[4]
[1]*University of Applied Sciences, 3100 St. Poelten, Austria*
[2]*Toyota Motor Corp., Toyota City, 471-8572, Japan*
[3]*Department of Geophysics, University of Muenchen, 80333 Munich, Germany*
[4]*Department of Physics, University of California, Davis, California 95616, USA*

(Presented 3 November 2011; received 23 September 2011; accepted 23 November 2011; published online 9 March 2012)

First order reversal curve (FORC) diagrams are a useful tool to analyze the magnetization processes in magnetic materials. FORC diagrams are computed from measured first order reversal curves on sintered $Nd_2Fe_{14}B$ magnets. It is shown that the FORC diagram simplifies if the first order reversal curves a desheared using the macroscopic demagnetizing field given by the geometry of the sample. Furthermore the resulting FORC diagram is almost identical to the FORC diagram measured for a thin platelet of the same material. This opens the possibility to compare experimental FORC diagrams with FORC diagrams computed by micromagnetic simulations.
 [doi:10.1063/1.3678434]

I. INTRODUCTION

Sintered NdFeB-based magnets give the highest energy density product.[1] Thus they have a wide application area whenever size or weight of the magnet becomes important. Analysis of the coercive field as function of temperature[2] indicate that magnetization reversal in sintered NdFeB-based magnets is governed by the nucleation and expansion of reversed domains. This proposition has not been confirmed yet by micromagnetic computation, which because of the huge grain size of sintered magnets, so far has been limited to two-dimensional simulations[3] or to studies of microstructural details such as grain boundary junctions.[4]

First order reversal curve (FORC) analysis is a useful tool to understand reversal mechanisms, switching field distributions, and interactions in magnetic systems.[5,6] In this paper we apply FORC analysis to sintered $Nd_2Fe_{14}B$-permanent magnets and compare experimentally obtained curves with micromagnetically computed ones.

II. MICROMAGNETIC AND NUMERICAL BACKGROUND

We apply finite element micromagnetic simulations[7] for the simulation of the hysteresis loop and the first order reversal curves of a sintered permanent magnet. The method is modified in order to take into account the different characteristic length scales in a sintered magnet. Firstly, the grain size of sintered magnets might well exceed 1 μm. Secondly, microstructural features in the order of 1 nm drastically influence the magnetization reversal process. Defects near the grain boundary with a size of around 0.5 nm to 2 nm play a critical role in magnetization reversal.[2] In order to treat the magnetostatic interactions and magnetization reversal in an ensemble of grains of a sintered magnet, we apply the following two techniques: (1) The demagnetizing field is evaluated by direction integration over the field sources at the boundaries of the grain. (2) We add an additional torque to compute the influence of soft magnetic defects on magnetization reversal.

The simulation of large grained materials is a challenge for conventional micromagnetic simulations. Based on computer experiments Rave *et al.*[8] found that the mesh size has to be smaller than the exchange length, in order to compute the nucleation field of a $Nd_2Fe_{14}B$ particle. In $Nd_2Fe_{14}B$ the exchange length is $\delta = (A/K)^{1/2} = 1.35$ nm. Here A is the exchange constant and K is the magnetocrystalline anisotropy constant. Therefore a small mesh size is required near the edges of the grains where a reversed domain will nucleate. Near the edges the modulus of the demagnetizing field, $\mathbf{H}_d$, reaches its maximum.[9] Near the edge the demagnetizing field as a strong transverse component and thus creates a torque on the magnetization. This leads to the well known flower state.[10] Near the edges the magnetization, $\mathbf{M}$, rotates outwards. An external field, $\mathbf{H}_{ext}$, will create an additional torque. The flower state becomes more pronounced when the external field is increased. Exchange interactions and magnetocrystalline anisotropy balance the torque created by $\mathbf{H}_d$ and $\mathbf{H}_{ext}$. When $\mathbf{H}_{ext}$ reaches the nucleation field a reversed nucleus is formed near the edge which is energetically more favorable. Rave *et al.*[8] looked into the individual contributions to the total torque near the edge. The demagnetizing field shows a singularity at the edge.[9] The finer the mesh, the closer $\mathbf{H}_d$ is evaluated near the edge. Therefore, flower state becomes more pronounced and the nucleation field decreases with finer mesh size. On the other hand, a smaller computational grid, leads to a higher local exchange field. At a grid size of $[1/2]\delta$ or smaller the torque from the demagnetizing field and the torque from the exchange field balance each other. A further mesh refinement of the mesh will not change the results.

[a)]Author to whom correspondence should be addressed. Electronic mail: thomas.schrefl@fhstp.ac.at.

The purpose of this study is to investigate magnetization reversal taking into account the interactions between many grains. A uniform fine grid or to a graded mesh that becomes smaller near the grain boundaries will lead to billions of unknowns, system sizes that are too large for available computational resources. We use the above findings to construct a micromagnetic algorithm that allows a uniform computational grid size which is orders of magnitude larger than δ. We solve the Landau-Lifhsitz Gilbert equation whereby the external field is a given function of time, in order to compute the loops and the reversal curves.

$$\frac{1+\alpha^2}{|\gamma|}\frac{\partial \mathbf{M}}{\partial t} = -\mathbf{M}\times\mathbf{H}_{\text{eff}} - \frac{\alpha}{M_s}\mathbf{M}\times\mathbf{M}\times\mathbf{H}_{\text{eff}}, \text{with}$$
$$\mathbf{H}_{\text{eff}} = \mathbf{H}_{\text{ext}}(t) + \mathbf{H}_{\text{ex}} + \mathbf{H}_{\text{d}} + \mathbf{H}_{\text{a}}. \quad (1)$$

M_s is the spontaneous magnetization. $\mathbf{M}$ is the magnetization and $\mathbf{H}_{\text{eff}}$ is the effective field. We apply a weak formulation for the computation of the exchange field, $\mathbf{H}_{\text{ex}}$, and the anisotropy field, $\mathbf{H}_{\text{a}}$, at the nodes of a tetrahedral grid.[7] The demagnetizing field at the integration points of the finite elements is computed from surface charges at the grain boundaries. We use the nodes of the grid as integration points except for nodes that are on grain boundaries. For these points the fields are evaluated at a distance of $[1/2]\delta$ from the grain boundaries. The field evaluation is accelerated using hierarchical matrices to evaluate the surface intergrals.[11]

A key feature that considerably influences the magnetization reversal process in sintered $Nd_2Fe_{14}B$ magnets are magnetically soft defects. Near the grain boundary the $N_2F_{14}B$ crystal lattice is distorted[12] and the magnetocrystalline anisotropy is close to zero. Thus magnetization reversal is very similar as in exchange-spring systems.[13] Reversal starts in the soft magnetic region. Because of the difference between the grain size and the thickness of the defect layer, we are not able to resolve the defects with the finite element mesh. Instead we add an additional torque to the nodes at the grain boundaries. The nucleation field of a hard magnet with a soft magnetic defect is given by[14]

$$H_{\text{n}} = \beta\frac{A}{t^2\mu_0 M_s}, \quad (2)$$

where β depends on the geometry and t is the thickness of the defect. If the local field, $H_{\text{d}} + H_{\text{ext}}$, exceeds H_{n} the magnetization will reverse. Then we modify the effective field for nodes near soft magnetic defects by

$$\mathbf{H}'_{\text{eff}} = \mathbf{H}_{\text{eff}} + \beta\frac{A}{t^2 M_s}\frac{(\mathbf{H}_{\text{ext}}+\mathbf{H}_{\text{d}})}{|\mathbf{H}_{\text{ext}}+\mathbf{H}_{\text{d}}|}. \quad (3)$$

The newly developed boundary integration method has been tested for a cubic $Nd_2Fe_{14}B$ particle. First the coercive field as function of particle size was calculated with conventional finite element micromagnetics. In order to account for the mesh size requirements[8] and the thin soft magnetic defects[2] we use a geometrically graded mesh that becomes finer toward the surface of the cube. Then the simulation was repeated using a uniform mesh and boundary integration method. Figure 1(a) compares the computed coercive field of the different methods. The thickness of the distorted layer with $K = 0$ is 0.8 nm. For a particle size of 300 nm the number of finite elements is 500 000 for the graded mesh and finite element method. For the uniform mesh and the boundary integration technique the number of elements is only 500. Thus we can model large scale multigrain structures with the new method.

The three-dimensional grain structure follows from a Voronoi-construction.[3] First a cube is divided into n^3 regular sub-cells. Within each cell we place a seed point for grain growth at a random position. Additional seed points that are mirrored at the magnets outer surface are added. Grain growth with an isotropic growth velocity leads to the grain structure. For the final finite element model only the grains inside the cubes are meshed into tetrahedral finite elements. The grains are separated by a 2 nm thin non-magnetic phase. Figure 1(b) shows the resulting grain structure and the finite element mesh.

III. RESULTS AND DISCUSSION

A set of first-order reversal curves measured on a sintered $Nd_2Fe_{14}B$ magnet of cubic shape is shown in Fig. 2(a). The corresponding FORC diagram of Fig. 2(b) exhibits a complex peak structure. To identify the inherent physics a deshearing is performed with a demagnetizing factor of $N = 0.33$ to create the FORC diagram that corresponds to a

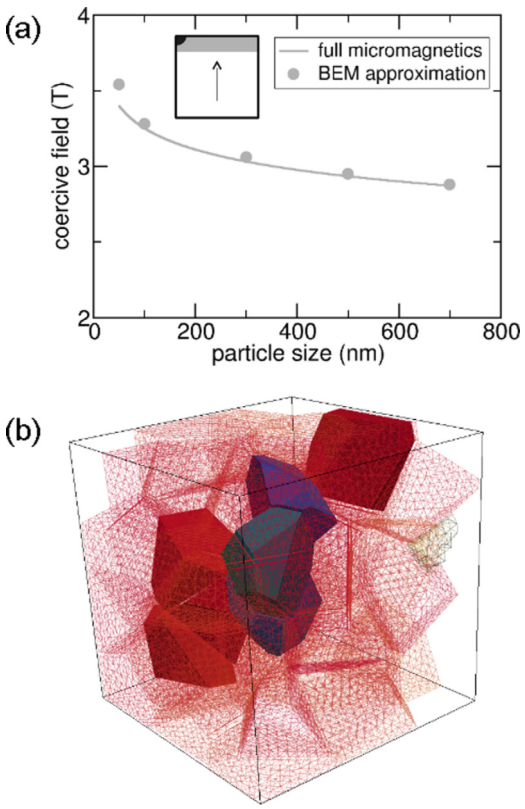

FIG. 1. (Color online) (a) Comparison of finite element micromagnetics on a graded mesh (solid line) with the boundary integration method (dots) for computing hysteresis properties. The plot gives the coercive field of a $Nd_2Fe_{14}B$ cubic sample as function of size. (b) Grain structure and finite element mesh of computer model of a sintered $Nd_2Fe_{14}B$ magnet.

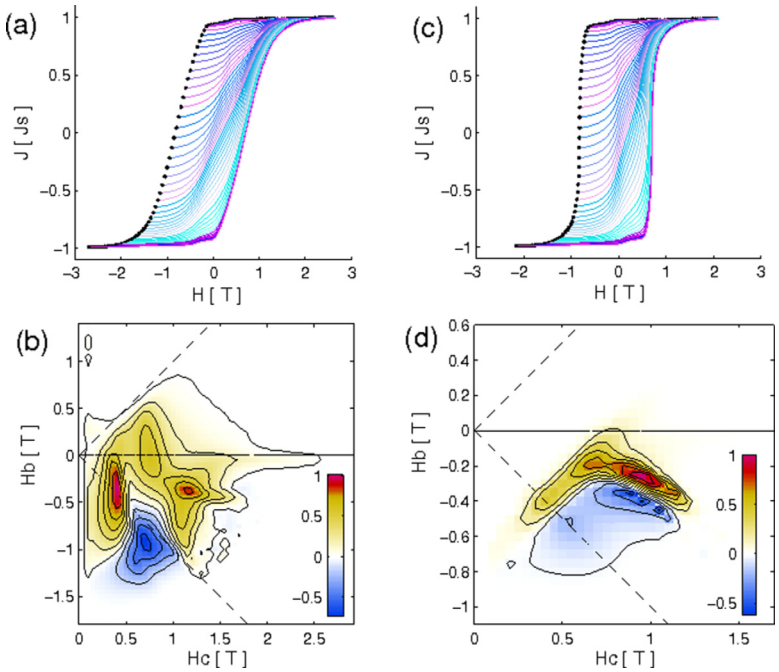

FIG. 2. (Color online) (a) First order reversal curves measured on a cubic $Nd_2Fe_{14}B$ magnet. (b) corresponding FORC diagram. (c) First order reversal curves desheared with a demagnetizing factor of $N = 0.33$; (d) corresponding FORC diagram.

platelet shaped sample as shown in Fig. 2(d). Remarkably the FORC of the platelet sample reveals a simple structure of a well defined peak broadened in two directions into a ridge in a correlated manner as captured by the curvature of the ridge, which yields itself to a much more transparent physical interpretation. Figure 2(d) closely resembles the FORC diagram measured for the same magnetic material directly in a platelet shape.

Figure 3 shows FORC curves simulated for a cubic sample. First order reversal curves were computed for 64 grains with a diameter of 1 μm. The first-order anisotropy constants K for each grain were taken randomly from a Gaussian distribution with a mean of $<K> = 4.2\,MJ/m^3$ and a $\sigma_K/<K>$ of 10%. The magnetization is $\mu_0 M_s = 1.61\,T$ and the exchange constant is $A = 7.7\ pJ/m^3$. The thickness of the distorted layer at grain boundaries is $t = 0.51\,nm$. The easy axes were uniformly distributed within a cone. The opening angle of the cone is adjusted in order to achieve a given degree of alignment f, where $f = \sum_{i=1}^{64} \cos(\theta_i)/64$ and θ_i is the misalignment angle of grain i. The first order reversal curves were averaged over 5 different realizations of K distributions and then desheared with a demagnetizing factor of $N = 0.33$ as the experimental FORCs. The resulting FORC diagrams are shown in Fig. 3. The resemblance between the measured and the simulated FORCs is striking, suggesting that the simulated model is capturing the physics of the experimental samples with high fidelity.

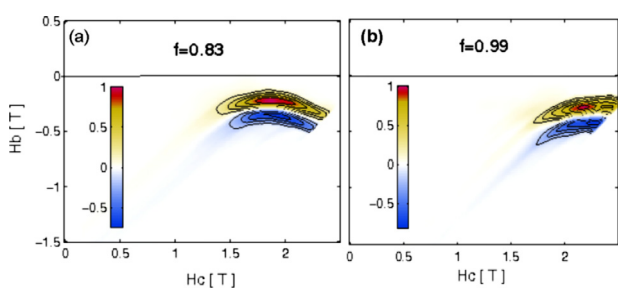

FIG. 3. (Color online) FORC diagram of a modeled sintered magnet with degree of alignment (a) $f = 0.83$ and (b) $f = 0.99$, with otherwise identical computation and processing parameters. The coercive force of the major hysteresis loop is (a) 1.7 T and (b) 2.1 T.

Figure 3(a) shows magnet with medium degree of alignment of $f = 0.83$ and Fig. 3(b) shows the result for a magnet with the same grain structure but an alignment of $f = 0.93$. Visibly, increasing alignment increased the average value of the coercivity distribution and decreased the width of this distribution, both of them desirable for improving magnet performance. Here a note of caution that our simulations do not include thermal fluctuations, which may lead to a lower average coercive field at better alignments.

ACKNOWLEDGMENTS

We gratefully acknowledge the financial support by Toyota Motor Corporation and the Austrian Science Fund (SFB F41).

[1]J. F. Herbst and J. J. Croat, J. Magn. Magn. Mater. **100**, 57 (1991).
[2]H. Kronmüller, K.-H. Durst, and M. Sagawa, J. Magn. Magn. Mater. **74**, 291 (1988).
[3]T. Schrefl and J. Fidler, J. Magn. Magn. Mater. **111**, 105 (1992).
[4]D. Suess, T. Schrefl, and J. Fidler, IEEE Trans. Magn. **36**, 3282 (2000).
[5]C. R. Pike, C. A. Ross, R. T. Scalettar, and G. Zimanyi, Phys. Rev. B **71**, 134407 (2005).
[6]M. Winklhofer and G. T. Zimanyi, J. Appl. Phys. **99**, 08E710 (2006).
[7]T. Schrefl, G. Hrkac, S. Bance, D. Suess, O. Ertl, J. Fidler, in *Handbook of Magnetism and Advanced Magnetic Materials*, edited by H. Kronmuller and S. Parkin, (John Wiley and Sons, 2007), Vol. 2, pp. 765–794.
[8]W. Rave, K. Ramstöck, and A. Hubert, J. Magn. Magn. Mater. **183**, 329 (1998).
[9]M. Grönefeld and H. Kronmüller, J. Magn. Magn. Mater. **80**, 223 (1989).
[10]M. E. Schabes and H. N. Bertram, J. Appl. Phys. **64**, 1347 (1988).
[11]L. Grasedyck and W. Hackbusch, Computing **70**, 295 (2003).
[12]G. Hrkac, T. G. Woodcock, C. Freeman, A. Goncharov, J. Dean, T. Schrefl, and O. Gutfleisch, Appl. Phys. Lett. **97**, 212511 (2010).
[13]E. Goto, N. Hayashi, T. Miyashita, and K. Nakagawa, J. Appl. Phys. **36**, 2951 (1965).
[14]R. Skomsi, J. Phys.: Condens. Matter **15**, R841 (2003).